Journal of Hydrology (2008) 362, 191–205

available at www.sciencedirect.com

ScienceDirect

journal homepage: www.elsevier.com/locate/jhydrol

Coupling of heat, water vapor, and liquid water fluxes to compute evaporation in bare soils

Marco Bittelli [a,*], Francesca Ventura [a], Gaylon S. Campbell [b], Richard L. Snyder [c], Fabia Gallegati [a], Paola Rossi Pisa [a]

[a] Department of AgroEnvironmental Science and Technology, University of Bologna, Viale Fanin, 44, 40125 Bologna, Italy
[b] Decagon Devices Inc., Pullman, WA, USA
[c] Department of Air, Land and Water Resources, University of California, Davis, CA, USA

Received 7 May 2007; received in revised form 8 January 2008; accepted 15 August 2008

KEYWORDS
Evaporation;
Coupled fluxes;
Soil water content;
Aerodynamic resistance;
Soil surface resistance

Summary The quantification of soil evaporation and of soil water content dynamics near the soil surface are critical in the physics of land-surface processes on regional and global scales, in particular in relation to mass and energy fluxes between the ground and the atmosphere. Although it is widely recognized that both liquid and gaseous water movement are fundamental factors in the quantification of soil heat flux and surface evaporation, their computation is still rarely considered in most models or practical applications. Moreover, questions remain about the correct computation of key factors such as the soil surface resistance or the soil surface temperature. This study was conducted to: (a) implement a fully coupled numerical model to solve the governing equations for liquid water, water vapor, and heat transport in bare soils, (b) test the numerical model with detailed measurements of soil temperature, heat flux, water content, and evaporation from the surface, and (c) test different formulations for the soil surface resistance parameter and test their effect on soil evaporation. The code implements a non-isothermal solution of the vapor flux equation that accounts for the thermally driven water vapor transport and phase changes. Simulated soil temperature, heat flux, and water content were in good agreement with measured values. The model showed that vapor transport plays a key role in soil mass and energy transfer and that vapor flow may induce sinusoidal variations in soil water content near the surface. Different results were obtained for evaporation calculations, depending on the choice of the soil surface resistance equation, which was shown to be a fundamental term in the soil–atmosphere interactions. The

* Corresponding author. Tel.: +39 051 2096656; fax: +39 051 2096241.
E-mail address: marco.bittelli@unibo.it (M. Bittelli).

0022-1694/$ - see front matter
doi:10.1016/j.jhydrol.2008.08.014

results also demonstrated that soil water dynamics are strongly linked to temperature variations and that it is important to consider coupled transport of heat, vapor and liquid water when assessing energy dynamics in soils.

Introduction

The movement of soil heat, water vapor, and liquid water at the land–atmosphere interface controls many processes in the physics of land-surface, including the mass and energy fluxes between the ground and the atmosphere, and fundamental biological processes such as seed germination and plant growth.

Early studies on the interactions between liquid water movement, water vapor transfer, and heat flux elucidated that the movement of heat and soil moisture are coupled (Taylor and Cavazza, 1954). Although thermal gradients affect liquid water redistribution of liquid water in soils, the most important process, which determines the coupling between water and heat, is the transport of latent heat by vapor flux within the soil and at the interface between the soil and the atmosphere. The works by Taylor and Cavazza (1954) and Philip and de Vries (1957) showed that, at high and intermediate soil water contents, vapor flux in response to thermal gradients was greater than predicted by Fick's law. For this reason, enhancement factors were introduced to account for the effects of thermal gradients on water vapor diffusion (Philip and de Vries, 1957; Cary, 1963, 1964; Rose, 1968a,b; Jackson et al., 1974; Jury and Letey, 1979). Based on Philip and de Vries (1957), Cass et al. (1984) proposed a theoretical examination of the enhancement factors and presented a comparison of different approaches. Jassal et al. (2003) presented a model for the simultaneous transport of heat and water in a bare soil; however, a detailed experimental verification of vapor flux above the soil surface was not provided.

Rose (1968b) discussed the possibility that convective mass flow of air through the soil could be an additional physical effect that may explain the disagreement between experimental results and theory. For his experimental conditions, however, the author concluded that convective mass flow accounted for only 0.1% of the total vapor flux. Following this idea, Cahill and Parlange (1998) and Parlange et al. (1998) proposed that the mechanisms for the large vapor flux is convective transport driven by the diurnal heating and cooling of the soil surface and the consequent thermal expansion and contraction of soil air. Their conclusion was based on the calculation of vapor flux using the residual of the mass transfer equation and the energy balance equation, and it was corroborated using diurnal fluctuations of soil water content. Moreover, inadequate correction of soil moisture measurements and calibration of sensors under different temperature regimes could also have led to the conclusions supporting their theory. Rose (1968b), however, pointed out the errors introduced in vapor flow calculations might also be due to: (1) lack of coupling in the computation of heat, liquid water, and vapor fluxes, (2) errors in the computation of the soil thermal conductivity, (3) errors in the computation of the soil hydraulic properties, and (4) difficulties in the determination of the resistance parameters at the soil–atmosphere interface.

Indeed, a very important component for evaporation is the correct formulation of the resistances to vapor flow at the interface between the soil surface and the atmosphere. The two main resistances are the soil surface resistance and the aerodynamic resistance which together, determines the total resistance term. Several works (Shu Fen Sun, 1982; Camillo and Gurney, 1986; Kondo et al., 1990; van de Griend and Owe, 1994) have proposed different equations to compute the soil surface resistance; however, parameterization of soil resistance is still unclear and the different equations provide very different results in terms of quantification of the evaporation, likely because they were derived for specific type of soils. Moreover, while it is widely accepted that the coupling of liquid water, water vapor, and heat flux is a fundamental factor in the quantification of soil evaporation, the computation is still rarely accounted for in models or practical applications. Saito et al. (2006) presented a numerical analysis of coupled water, vapor, and heat transport in soils; however, in their work there is no independent experimental test of evaporation, because the energy budget terms are used as upper boundary conditions for the soil's numerical model.

In this work, the problem is approached by using: (1) an implementation of a fully coupled numerical model to solve for heat flux, liquid water movement, vapor flux in the soil and at the soil–atmosphere interface, (2) a test of the model through an independent direct measurement of evaporation, soil heat flux, soil moisture, and soil temperature, and (3) a comparison between different equations for computing the soil resistance term, and the evaluation of their effect on simulated evaporation.

Transport equations

Heat transport

The transport of heat in soils is described as

$$q_h = -\lambda \nabla T + L q_v \quad (1)$$

where q_h is the heat flux density (W m^{-2}), λ is the thermal conductivity (W m^{-1} K^{-1}), T is temperature (K), L is the latent heat of vaporization ($\approx 2.45 \times 10^6$ J kg^{-1}) and q_v is vapor flow (kg m^{-2} s^{-1}). The first term on the right-hand side describes heat transfer by conduction (sensible heat) and the second term describes heat transfer by water vapor flux (latent heat).

Vapor transport

The isothermal, vertical transport of water vapor is given by Fick's law:

$$q_v^i = -D_v \frac{dc_v}{dz} \tag{2}$$

where D_v is the vapor diffusivity in soil ($m^2\ s^{-1}$), and c_v is the soil vapor concentration ($g\ m^{-3}$). Vapor concentration is obtained by

$$c_v = h c_v' \tag{3}$$

where h is the fractional relative humidity and c_v' is the saturation vapor concentration. If the soil is isothermal, the variation of vapor concentration with depth can be written as

$$\frac{dc_v}{dz} = c_v' \frac{dh}{dz} \tag{4}$$

The partial pressure of water vapor is related to the soil water potential through the fractional relative humidity:

$$h = \exp\left(\frac{M_w \psi}{RT}\right) \tag{5}$$

where M_w is the molecular weight of water (0.018 $kg\ mol^{-1}$), ψ is the soil water potential ($J\ kg^{-1}$), R is the gas constant (8.31 $J\ mol^{-1}\ K^{-1}$) and T is temperature (K). Substituting these expressions into Eq. (2), vapor flow can be written as

$$q_v^i = -k_v \frac{d\psi}{dz} \tag{6}$$

where

$$k_v = \frac{D_v c_v' h M_w}{RT} \tag{7}$$

is the water vapor conductivity. This description of vapor flow only accounts for vapor concentration gradients. A more general analysis of soil evaporation must include the effects of temperature gradients on water transport. Non-isothermal vapor flow is described by

$$q_v^* = q_v^i + q_v^T = -D_v c_v' \frac{dh}{dz} - D_v h s \frac{dT}{dz} \tag{8}$$

where q_v^* is non-isothermal vapor flow, q_v^i is isothermal vapor flow (equivalent to Eq. (2)) and q_v^T is the thermally driven vapor flow, which can be written as

$$q_v^T = -D_v h s \frac{dT}{dz} \tag{9}$$

where s is the slope of the saturation vapor concentration function ($s = \Delta/P$), Δ is the slope of the saturation vapor pressure curve at temperature T, and P (kPa) is the barometric pressure. Using the equation of Buck (1981) for the saturation vapor pressure at temperature T,

$$e_s(T) = 0.611 \exp\left(\frac{17.27T}{T + 237.3}\right) \tag{10}$$

the slope of the saturation vapor pressure ($kPa\ K^{-1}$) over liquid water at temperature T is given by

$$\Delta = \frac{4098 e_s}{(T + 237.3)^2} \tag{11}$$

Liquid water transport

The transport of liquid water is described by the Richards' equation:

$$\frac{\partial \theta}{\partial t} = \nabla \bullet \{K(\psi_m)[\nabla \psi_m + g\hat{\mathbf{z}}]\} \tag{12}$$

where θ ($m^3\ m^{-3}$) is the volumetric water content, ψ_m ($J\ kg^{-1}$) is the matric potential, K ($kg\ s\ m^{-3}$) is the hydraulic conductivity, t is the time (s), g is the acceleration due to gravity, $\hat{\mathbf{z}}$ is the unit vector in vertical direction with positive upwards.

Eq. (12) is also referred as the mixed form of Richards' equation because water content and matric potential occur simultaneously. Eq. (12) is a second-order, nonlinear partial differential equation, which is generally solved by numerical methods. The strong nonlinearity of Richard's equation is due to the highly nonlinear dependency of the hydraulic properties, *e.g.*, the dependency of the hydraulic conductivity on the pressure head.

Soil parameters

Hydraulic properties

Campbell's equation (Campbell and Shiozawa, 1992) was used to characterize the soil hydraulic properties:

$$\theta = \begin{cases} \theta_s \left(\frac{\psi_m}{\psi_e}\right)^{-1/b} & \text{if } (\psi_m < \psi_e) \\ \theta_s & \text{if } (\psi_m \geqslant \psi_e) \end{cases} \tag{13}$$

where ψ_m ($J\ kg^{-1}$) is the matric potential, ψ_e ($J\ kg^{-1}$) is the air entry potential, θ ($m^3\ m^{-3}$) is the volumetric water content, θ_s ($m^3\ m^{-3}$) is the saturated volumetric water content, and b is a shape parameter, which is related to the pore size distribution of the porous media. The hydraulic conductivity function is given by

$$K = \begin{cases} K_s \left(\frac{\psi_e}{\psi_m}\right)^{\left(2+\frac{3}{b}\right)} & \text{if } (\psi_m < \psi_e) \\ K_s & \text{if } (\psi_m \geqslant \psi_e) \end{cases} \tag{14}$$

where K ($kg\ s\ m^{-3}$) is the unsaturated hydraulic conductivity and K_s ($kg\ s\ m^{-3}$) is the saturated hydraulic conductivity. Since no direct measurement of the soil hydraulic properties was performed, the soil moisture characteristics and the hydraulic conductivity functions were derived using pedotransfer functions (Campbell and Shiozawa, 1992) and measured soil texture (% of sand, silt and clay) and bulk density. Following Grismer et al. (1995), permeability and available water holding capacity were measured and used to evaluate estimation of the soil hydraulic parameters. Good agreement between the estimated and measured parameters was observed.

Thermal properties

Following de Vries (1963), a modified model proposed by Campbell et al. (1988), was used to determine apparent soil thermal conductivity. The apparent thermal conductivity (λ) is given by

$$\lambda = \frac{k_w \theta \lambda_w + k_a x_a \lambda_a + k_m x_m \lambda_m}{k_w \theta + k_a x_a + k_m x_m} \tag{15}$$

In this equation, the soil is considered as a mixture of water, gas and solid materials having volumetric fractions, θ, x_a and x_m, respectively. Each component has a thermal

conductivity, λ_w (water), λ_a (air) and λ_m (mineral), and the k_w, k_a, and k_m are the respective weighting factors. Computation of the weighting factors is described in Campbell et al. (1988). The thermal conductivity of the gas phase, λ_a, is described by the sum of the thermal conductivity for conduction through air and the latent heat of distillation across pores. The improvement provided by using this model, in respect to the original de Vries (1963) model, is that temperature dependence of the thermal conductivity is accounted. Since the temperature dependence of the soil apparent thermal conductivity is primarily due to changes in the latent heat of vaporization with temperature, this effect has a relevant role on vapor flow calculations and therefore on evaporation calculations.

Vapor properties

The gas diffusivity through a porous medium is described as the product of the binary diffusion coefficient for the specific gas in air and a function that accounts for the fraction of pores that are air-filled (air-filled porosity). The binary diffusion coefficient for a gas, which depends on pressure and temperature, is expressed as

$$D_0(T,P) = D_0(273.15\ \mathrm{K}, 101.3\ \mathrm{kPa})\left(\frac{T}{273.15}\right)^{1.75}\left(\frac{101.3}{P}\right) \tag{16}$$

where D_0 (273.15 K, 101.3 kPa) = 2.12×10^{-5} ($m^2\ s^{-1}$), for water vapor in the gas phase. The diffusivity of gases in liquid water is much smaller (about $2 \times 10^{-9}\ m^2\ s^{-1}$) and the gas exchange in soils without a continuous gas phase is negligible (Campbell, 1985). Consequently, gas transport through liquid water is not considered in this work. Soil vapor diffusivity (D_v) is given by

$$D_v = D_0 \varepsilon(x_a) \tag{17}$$

where ε (x_a) is a soil parameter that depends on the air-filled porosity (x_a) and on soil geometrical properties.

When soil saturates, ε (x_a) goes to zero and no vapor flow occurs. The air-filled porosity is computed as the difference between water content at saturation (θ_s) and actual water content (θ). The actual water content is updated in the code for each time and space iteration. The parameter ε (x_a) is given by

$$\varepsilon(x_a) = \beta x_a^m \tag{18}$$

where β and m are empirical parameters that depends on the shape of the soil particles. Values of $\beta = 0.9$ and $m = 2.3$ were used in this simulations.

Evaporation equation, aerodynamic resistance and soil surface resistance

It is well known that soil evaporation (E) rates follow a three-stage process (Feddes, 1971; Idso et al., 1974). During the first stage, the evaporation rate is only limited by the amount of energy available to vaporize soil moisture in the upper layer of the soil and by the vapor pressure deficit between the surface and the air, and it is similar to evaporation from a surface of free water. This phase ends when the soil moisture content in the upper layer decreases and the soil matric potential becomes more negative.

During the second stage, evaporation is limited by soil hydraulic properties that determine the transfer of liquid and vaporized water to the surface. In this stage, the water moves in both the liquid and vapor forms. Stage-2 ends when there is minimal liquid water movement and water transfer is mainly due to vapor flux through the soil pores.

The third stage is determined mainly by soil physical characteristics. Evaporation rates are low in stage-3. Evaporation rates are high but short-lived during stage-1 (i.e., 1–3 days), so most evaporation in arid regions occurs during stage-2 (Brutsaert and Chen, 1995; Snyder et al., 2000; Ventura et al., 2001). Therefore, a good evaporation model requires accurate estimates mainly during stage-1 and stage-2. The distinction between these stages depends on the behavior of the resistance terms involved in evaporation calculations, and the dynamical changes of the soil moisture and temperature in the most superficial layers.

In this work, computation of evaporation is based on the water vapor transport equation, driven by the vapor concentration gradient between the atmosphere and the soil surface:

$$E = \frac{1}{r_v + r_s}\left(\frac{c_{va} - c_{vs}}{z_{ref} - z_0}\right) \tag{19}$$

where E is the evaporation rate ($kg\ m^{-2}\ s^{-2}$), r_v is the aerodynamic resistance for water vapor transfer ($s\ m^{-1}$), r_s is the soil surface resistance for water vapor transfer ($s\ m^{-1}$), c_{va} is the atmosphere vapor concentration at height (z_{ref}) ($mol\ mol^{-1}$), c_{vs} is the vapor concentration of the soil surface (z_0, T_s) ($mol\ mol^{-1}$). In this work, atmospheric relative humidity and air temperature were measured, while vapor pressures of the soil surface layers were computed by knowledge of the soil water potentials, using Eq. (5), where T is the soil surface temperature T_s. To convert the resistance terms for vapor, from $s\ m^{-1}$ to $m^2\ s\ mol^{-1}$, it is necessary to divide by the molar volume of air (41.4 mol m^3, at sea level and 20 °C), while to convert $m^2\ s\ mol^{-1}$ to $m^2\ s\ kg^{-1}$, it is necessary to divide by the molecular weight of water (0.018 $kg\ mol^{-1}$). These transformations allow one to compute the vapor flux in $kg\ m^{-2}\ s^{-1}$. Finally, this value was multiplied by 3600 s, to obtain the evaporation rate in $mm\ h^{-1}$.

The aerodynamic resistance for heat (r_H) and vapor (r_v) transport depends on surface roughness properties and wind speed (Campbell, 1977). Heat and vapor transport between the surface and some measurement height z_{ref} is given by

$$r_H = r_v = \frac{1}{u^* k}\left[\ln\left(\frac{z_{ref} - d + z_H}{z_H}\right) + \phi_H\right] \tag{20}$$

where u^* is the friction velocity ($m\ s^{-1}$), k is the von Karman's constant (with value = 0.41), z_{ref} is the reference height of temperature measurement (m), z_H is the surface roughness parameter for the heat flux (m), d is the zero plane displacement (m) and φ_H is the atmospheric stability correction factor for the heat flux. This equation assumes that the resistances to heat and vapor flux are roughly equal (Flerchinger et al., 1996). Friction velocity is defined as

$$u^* = uk\left[\ln\left(\frac{z_{ref} - d - z_M}{z_M}\right) + \phi_M\right] \tag{21}$$

where u is wind speed (m s^{-1}) at height z_{ref}, z_M is the surface roughness for the momentum flux, and φ_M is the atmospheric stability correction factor for momentum flux. A typical value for soil surface roughness is 0.01 m, which was used here for calculating r_v (Campbell and Norman, 1998). To calculate Φ_M and Φ_H, we used the stability function (Webb, 1977):

$$\phi_H = \phi_M = -\xi f \tag{22}$$

where $\xi = (z - z_M - d)/\Lambda$, with Λ being the Monin–Obukhov's stability parameter, and f is a constant (4.7 in this study). The stability parameter is computed as

$$\Lambda = \frac{u^{*3} Ch T_a}{kgH} \tag{23}$$

where Ch is volumetric heat of air (1200 J m^{-3} C^{-1} at 20 °C, at sea level), T_a is air temperature, g is the gravitational constant and k is the von Karman constant. While the semi-logarithmic wind profile law gives a fair estimate of the aerodynamic resistance (Tennekes, 1973), the computation of soil resistance is difficult and it has been object of several studies.

Camillo and Gurney (1986) and Kondo et al. (1990) reported that using only the aerodynamic resistance induces overestimation for dry soils because of the assumption of equilibrium in Eq. (5). When the soil is very dry, vapor is moved across large pores and it is not necessarily in equilibrium with the soil water content of the soil surface layer, suggesting the use of an additional resistance terms for soil surface resistance. This term is similar to the stomatal resistance in the computation of resistances for vegetation. Shu Fen Sun (1982) proposed an equation accounting for soil water content with a power term: $rs = 3.5 * (\theta_s/\theta_{top})^{2.3} + 33.5$.

Camillo and Gurney (1986) proposed a linear equation for r_s (s m^{-1}) taking into account the actual volumetric soil moisture (θ_{top}) and the saturated volumetric soil moisture (θ_s), of the first 1 cm top surface layer: $rs = -805 + 4140 * (\theta_s - \theta_{top})$. Both equations describe an increase in soil surface resistance with decreasing soil water content (Figure 14 in Camillo and Gurney, 1986).

van de Griend and Owe (1994), based on measurements of r_s using a fast circulation chamber, proposed an exponential law: $r_s = 10e^{0.3563(\theta_{min} - \theta_{top})}$, where θ_{top} (%) is the water content of the top 1 cm layer and θ_{min} (%) is an empirical minimum above which the soil is able to deliver vapor at a potential rate (θ_{min} = 15%, in their work). The factor 10 was obtained from studies of molecular diffusion of water surfaces (La Mer and Healy, 1965). In this work, the value of θ_{top} for the first 1 cm layer was dynamically computed by the numerical code, therefore allowing to change the surface resistance parameter with changing water content, while the θ_s is a constant.

van de Griend and Owe (1994) also pointed out that a correct computation of soil resistance must take into account the deepening of the evaporative front, therefore adding to the soil surface resistance additional resistances in series, corresponding to the resistances of the drying soil layers (Fig. 1 in their paper). In this work, soil vapor resistances

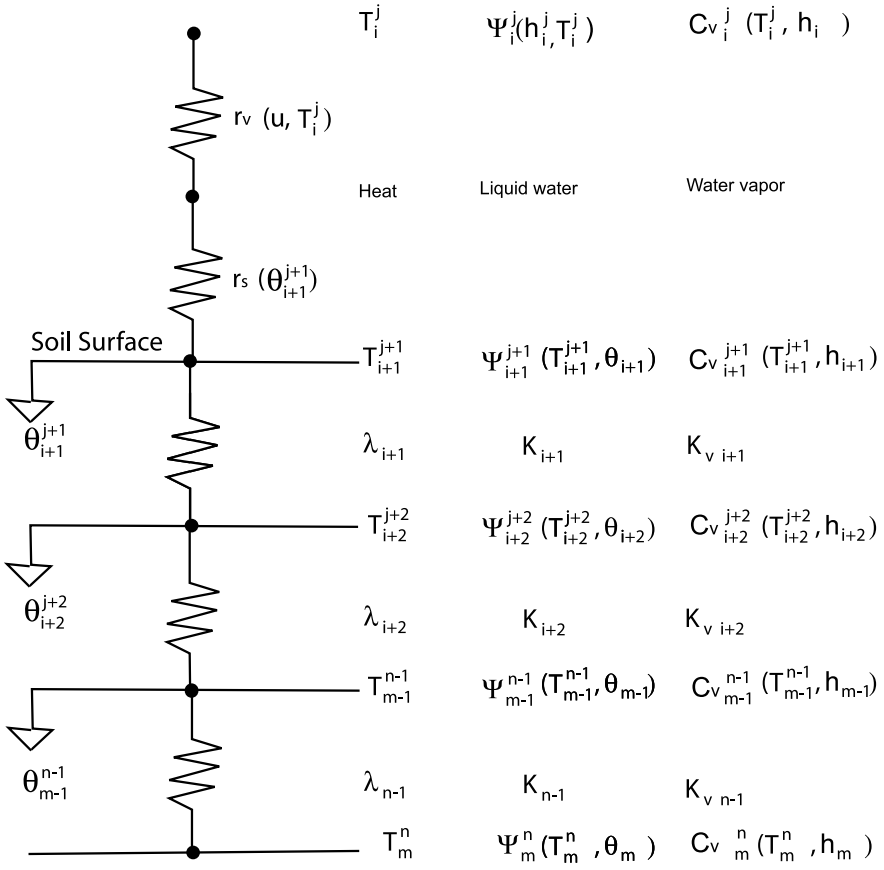

Figure 1 Scheme of the computational grid with the driving force terms (temperature, soil water potential and soil vapor concentration), the soil conductivities and the resistances involved at the soil–atmosphere interface.

(or conductivites) for each soil layers were computed by the numerical algorithm (Eqs. (7)–(10)), therefore accounting for all the necessary resistive terms, and for the driving vapor pressure differences. As described by van de Griend and Owe (1994), these computations are necessary to quantify vapor flow from the soil into the atmosphere and to determine the deepening of the soil evaporative front with time. In this work we also compared the three different equations for r_s, to investigate their effect on evaporation and identify the most suitable one for our experiment.

Soil surface temperature

Another limitation when using Eq. (19), is to obtain a reliable value of soil surface temperature (T_s), needed to compute the soil surface relative humidity (h_s) from soil surface water potential (Eq. (5)). Eq. (5) shows that for the same value of soil water potential, at a higher soil surface temperature there will be a higher soil surface relative humidity (the water potential has a negative value in the Eq. (5)) and, for the same atmospheric vapor pressure, there will be a smaller vapor pressure gradient between the atmosphere and the soil surface, affecting evaporation rates. For instance, under the same soil water potential conditions, if soil surface temperature is underestimated, evaporation rates are overestimated. Soil surface temperature has also been used as a proxy to compute soil evaporation by using the temperature differential between the soil surface temperature under a dry and a wet soil conditions, instead of the sensible heat flux (Guo Yu et al., 1999). Using this method the author proposed an evaporation transfer coefficient that replaced the aerodynamic resistance term. However, in their work the soil surface resistance term is not considered and evaporation is overestimated. Using a numerical solution of heat flow allow to obtain reliable values of soil surface temperature, by using thin (1 mm) computational layers at the top. In this work hourly values of air temperature were available, which were used as upper boundary condition for soil temperature, when daily maximum and minimum temperature only are available, it is possible to use trigonometric functions with a period of 24 h (Campbell, 1985).

Numerical implementation

Fig. 1 shows a scheme indicating the coupling of the driving terms (temperature, liquid water and vapor concentration) and the resistive and conductive terms. In the model, computer code, surface boundary conditions were set using the measured atmospheric boundary conditions (i.e., air temperature, vapor pressure and radiant energy). For the computation of liquid water flow, specified soil water potential boundary conditions were set during an irrigation period, by setting the upper computational layer at a water potential $\psi_m = \psi_e$, as specified in Eq. (13). After the end of the irrigation the upper boundary condition was variable water potential. The computed water potentials and temperatures of the soil surface layers were used to calculate the relative humidity (therefore the vapor pressure) used for vapor flow calculations (Eq. (5)). Free drainage (unit gradient) boundary conditions were set at the lower boundary, since the water table was far below the 1 m depth, set at lower boundary for the numerical experiment. The simulation was performed for 360 h (15 days) corresponding to the experiment duration. A time step of 1 h was used both for the simulation and the experimental data collection. After implementation of the initial and boundary conditions, the program simultaneously solved for the liquid water, water vapor, and heat fluxes.

The flow region is one-dimensional with total length z = 100 cm divided into 100 elements. To improve the precision of the numerical solution in the surface layers (relevant for computation of evaporation) the first two centimeters of soil were discretized into 10 layers of 0.2 cm depth, therefore using a finer grid near the surface. A Crank–Nicholson scheme was used (Ames, 1992). The mass balance equation for heat flow at a node is (Campbell, 1985)

$$\frac{(\lambda_i T_i - \lambda_{i-1} T_{i-1})}{(z_i - z_{i-1})} - \frac{(\lambda_{i+1} T_{i+1} - \lambda_i T_i)}{(z_{i+1} - z_i)} = \frac{C_h (T_i^{j+1} - T_i^j)(z_{i+1} - z_{i-1})}{2\Delta t} \quad (26)$$

where λ is the element thermal conductivity, T is the node temperature and C_h is the node heat capacity. The subscript i identifies the node, and the superscript j indicates time. Similarly, the mass balance equation for water flux at a node is

$$\frac{(K_i\psi_i - K_{i-1}\psi_{i-1})}{(z_i - z_{i-1})} - \frac{(K_{i+1}\psi_{i+1} - K_i\psi_i)}{(z_{i+1} - z_i)} - g(K_{i-1} - K_i) = \frac{\rho(\theta_i^{j+1} - \theta_i^j)(z_{i+1} - z_{i-1})}{2\Delta t} \quad (27)$$

where $K(\psi)$ is the element hydraulic conductivity, ψ is the node water potential, θ is the node water content, g is the gravitational constant and ρ is water density (1000 kg m^{-3} at 4 C). Eqs. (26) and (27) are mass balance equations where the right side is the change in heat or water content at position x_i over the time period Δt, and the left side is the difference between influx and outflux to and from the computational element, which depends on the temperature and water potential gradient. Mass balance equations similar to Eqs. (26) and (27) were written to solve for vapor flux (Campbell, 1985).

Numerical solutions of Eqs. (26) and (27) were obtained by using a Newton–Raphson (NR) algorithm for the nonlinear difference equations for heat, liquid water and vapor flow. The NR algorithm is a robust numerical solution (Paniconi and Putti, 1994), where the jacobian matrix is tridiagonal, and consequently a Thomas algorithm can be used (Press et al., 1992). The advantage from using the NR algorithm are the numerical robustness and the non-dependence of the algorithm to the time-step choice that can be much larger without any stability restriction on Δt (Morton and Mayers, 1994). The NR algorithm requires that iterations find new values for $\Delta\psi$ and ΔT, thereby reducing the mass balance error for that node. This feature allows a full coupling of the different flow phenomena at each time step because the solver simultaneously computes new values of node temperature, water content, and vapor concentrations. Iteration continues until the mass and heat balance are within a specified limit. In this work, the maximum allowable limit was 10^{-6} kg m^{-2} s^{-1} for liquid and vapor water fluxes, and 10^{-8} W m^{-2} for heat fluxes.

Table 1 Soil properties of the Imperial-Glenbar silty clay loam

Soil property	Value
Mass sand (kg kg^{-1})	0.4
Mass silt (kg kg^{-1})	0.4
Mass clay (kg kg^{-1})	0.2
Bulk density (kg m^3)	1160
Air entry potential (J kg^{-1})	−2.3
b value (−)	4.8
θ_s (m^3 m^{-3})	0.56
K_s (kg s m^{-3})	$7.41 * 10^{-3}$

The mass of sand, silt and clay as well as the bulk density were measured. The parameters for the hydraulic properties were estimated using pedo-transfer functions (Campbell and Shiozawa, 1992).

Methods and materials

A field trial was conducted at the University of California Desert Research and Extension Center (UCDREC) near Holtville, California during the period 2–17 October, 2003 to study soil dynamics during a drying cycle over a bare soil. The soil was an Imperial-Glenbar silty clay loam classified as fine, montmorrolinitic (calcareous) hypertermic Vertic Torrifluvens. The soil has moderately slow permeability (1.5–5.1 mm h^{-1}) and high available water-holding capacity (0.17–0.35 m^3 m^{-3}) (Grismer et al., 1995). Table 1 shows the hydraulic properties used for the numerical solution. The dimensions of the plots were 50×100 m^2 and the irrigation was applied on four adjacent plots for a total flooding area of 250×100 m^2 to minimize advection from fields around the experimental station.

Approximately 100 mm of water (typical irrigation for the region) was applied in a single surface irrigation event between 12:30 h and 16:00 h PST (Pacific Standard Time) on October 2, 2003. There was no rainfall during the field experiment. The second stage evaporation was reached on 9 October at 11:00 h (Ventura et al., 2006).

Soil measurements

Volumetric soil moisture (θ) was measured using four soil moisture sensors (ECH_2O probes from Decagon Devices Inc.). The probes are shaped similar to a 30 cm long meter stick (1 foot ruler) that is about 3 cm wide, and they were set horizontally lengthwise in a trench, with the sensor's face vertical in the soil to avoid water standing on the probe surface after the irrigation. One probe was set with the midpoint at 2.0 cm and a second was set with the midpoint at 5.5 cm depth below the surface. The sensors are about 3 cm wide, so the 2.0 cm sensor spanned the depth 0.5–3.5 cm and the 5.5 cm sensor spanned the depth 4.0–7.0 cm. Gravimetric samples were taken daily to calibrate the ECH_2O probes. Soil moisture measurements were continuously performed for 15 days to obtain a wide range of soil moisture (from 5% to 40%), ensuring a good calibration. The bulk density was measured as 1.16 g cm^{-3}.

The soil profile was monitored with soil heat flux sensors (HFT3-L REBS, Inc.) at depths of 2 and 7 cm below the surface. Thermocouples (TCAV-L, Campbell Sci. Inc.) were placed at 1, 3 and 7 cm below the surface to measure temperature.

Meteorological measurements and calculations

Meteorological data (precipitation, wind speed and solar radiation) were available on an hourly basis from the California Irrigation Management Information System (CIMIS) station (Snyder and Pruitt, 1992) that was located over irrigated grass at the UCDREC. Hourly air temperature and relative humidity were measured at the experimental station (over the bare soil). Fig. 2 shows the measured and solar irradiance, air temperature, and relative humidity from the CIMIS station and the net radiation measured over bare soil at the experimental site.

Evaporation measurements

An independent measure of soil evaporation (E_s) was determined using energy balance data including net radiation (R_n), soil heat flux density (G) and sensible heat flux density (H). Sensible heat flux density was determined using the surface renewal method (Paw U and Brunet, 1991; Paw U et al., 1995; Snyder et al., 1996, 1997; Spano et al., 1997), which uses high frequency temperature measurements above a surface and structure functions to determine ramp-like features that are characteristic of the temperature traces. The ramp amplitude and duration are used to estimate sensible heat flux density. The theory of the surface renewal technique was reviewed in detail by Paw U et al. (2005). Sensible heat flux density was calculated as

$$H' = \rho_a C_p \frac{a}{d+s} z \tag{28}$$

where ρ_a is the density of air, C_p is the specific heat of air at constant pressure, a is the ramp amplitude (°C), $d + s$ is the inverse ramp frequency or duration between ramps (s) and z is the measurement height (m). A calibration factor (α) that accounts for uneven heating below the temperature measurement height was determined by regression through the origin of H from a sonic anemometer versus H', so $H \approx \alpha H'$. Soil evaporation was determined from the latent heat flux density (LE), which was calculated as the residual of the energy balance equation:

$$\mathrm{LE} = R_n - G - H \tag{29}$$

where all variables are in W m^{-2}. Half-hourly data were averaged to determine hourly LE (MJ m^{-2} h^{-1}) and the means were divided by the latent heat of vaporization ($L \approx 2.45$ MJ m^{-2} mm^{-1}) to obtain E in mm h^{-1}.

Results and discussion

Soil temperature and heat flux

The sign of the convective and latent heat flux is positive when energy is transferred downwards into the soil. The fluxes are negative in the upward direction. Soil temperature and heat flux were simulated from 2 to 17 October 2003. Fig. 3a shows simulated and observed soil tempera-

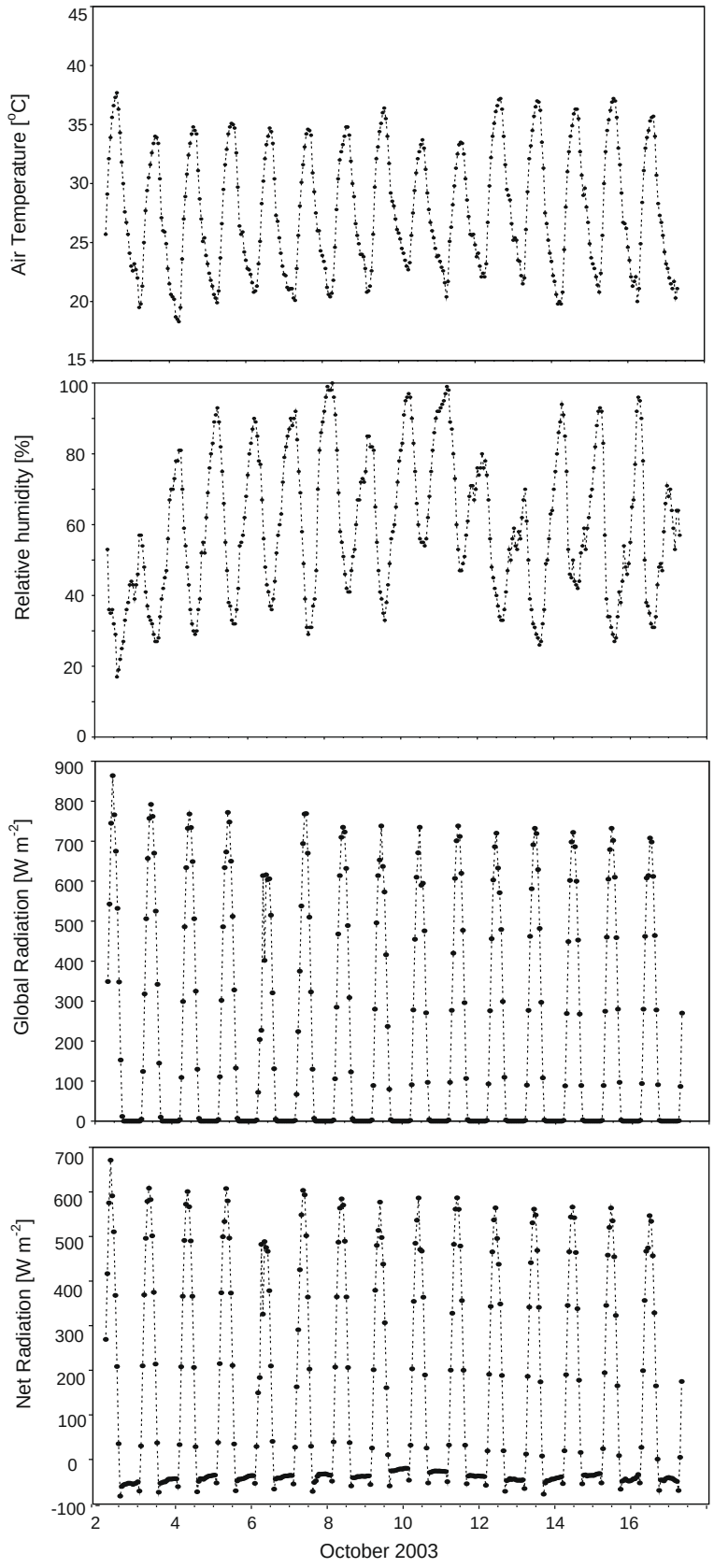

Figure 2 Air temperature, relative humidity, global radiation from the nearby CIMIS station and net radiation measured over soil at the experimental plot.

ture while Fig. 3b shows soil heat flux, as a function of time for the 2 cm depth. Soil temperature and heat flux density were well predicted by the numerical model. A comparison between observed and modeled temperatures gave a Root Mean Squared Error (RMSE) of 1.8 °C for the 2.0 cm depth, and 1.6 °C for the 5.5 cm depth, while a comparison between observed and modeled heat fluxes gave a RMSE of 20.1 W m^{-2} for the 2.0 cm depth and 11.2 W m^{-2} for the 5.5 cm depth. The experimental and simulated temperatures showed typical diurnal sinusoidal behavior with decreasing amplitude and delayed time of maximum and minimum with depth.

To analyze the contributions of conduction and latent heat transfer, model iteration of Eq. (1) was used to compute conductive and latent soil heat fluxes. The results for 2 cm depth are shown in Fig. 4. Large positive conduction from the solar-heated surface soil and negative latent heat flux were observed during daylight hours as the soil layer was loosing water vapor to evaporation from the surface. During nighttime, there was negative conduction to the cooler soil surface, whereas the latent term was positive because of condensation. During the course of the experiment, while the soil is drying, the latent heat component during night time increased, due to a higher condensation, since the soil surface was at a lower vapor pressure. The average daytime soil heat contribution from vapor flux at 2 cm depth, was on the order of 20 W m^{-2} (ranging from 2 to 63 W m^{-2}), which agrees with the results of Cahill and Parlange (1998). In general, these results confirm that latent heat flux has a major role in the soil energy budget, and it cannot be neglected.

Soil liquid water flux

Fig. 5 shows a time series of measured and simulated soil water content for the two measurement depths. The initial sharp increase in soil water content on 2nd October was due the irrigation at the beginning of the experiment (Ventura et al., 2006). After irrigation, the soil water content decreased from 0.49 to 0.05 m^3 m^{-3} in the upper layer (2.0 cm depth), whereas it decreased from 0.33 to 0.26 m^3 m^{-3} in the lower layer (5.5 cm depth). The numerical model gave good predictions of soil water content; especially considering the very sharp gradient of soil water content within the upper 6 cm of the soil surface. A comparison between observed and modeled soil moistures gave a RMSE of 0.04 m^3 m^{-3} for the 2.0 cm depth, and 0.02 m^3 m^{-3} for the 5.5 cm depth. The water content sensor has a

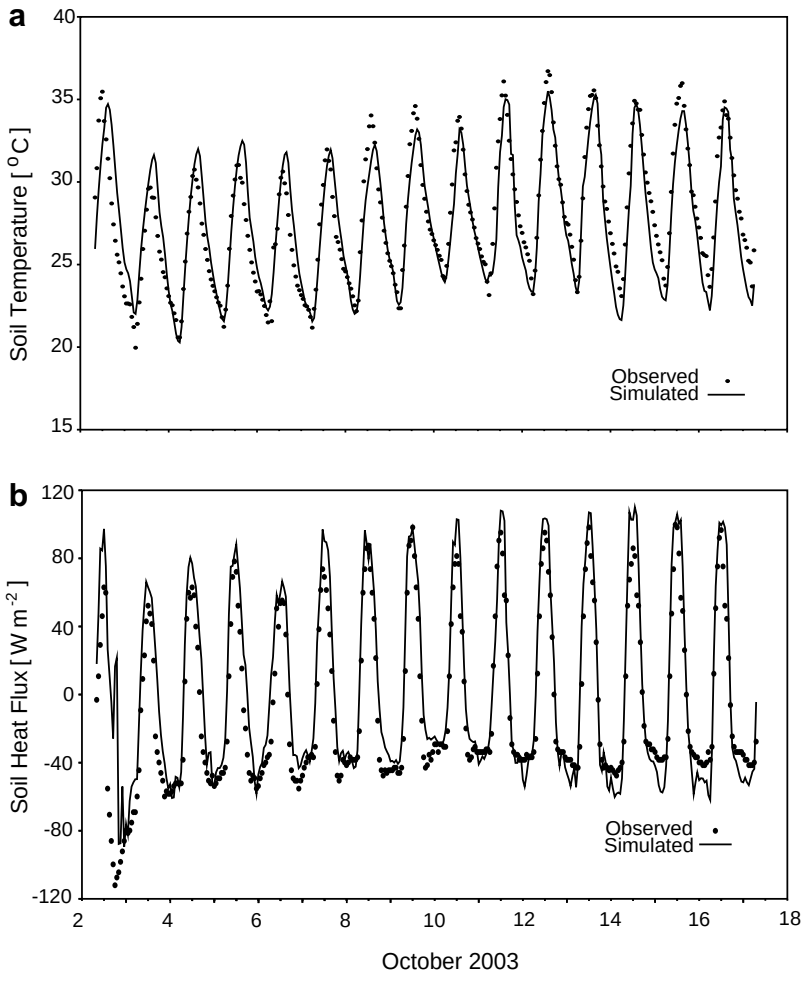

Figure 3 Simulated and measured soil temperatures and soil heat fluxes at 2.0 cm depth, as function of time.

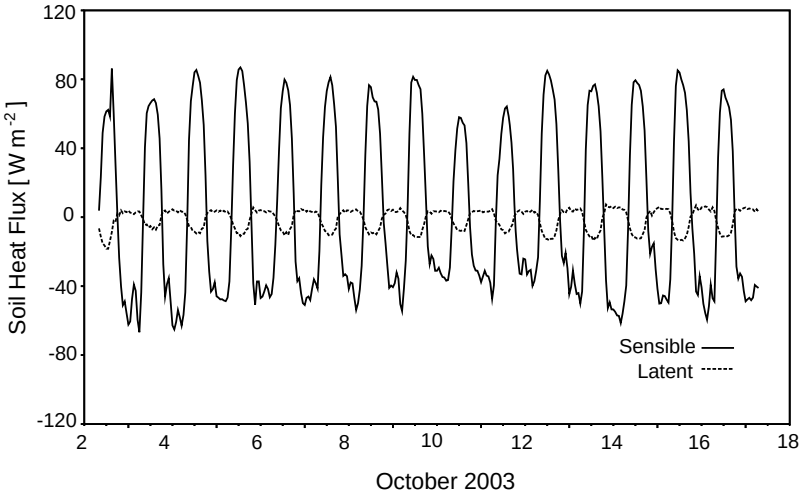

Figure 4 Simulated energy flux due to conduction (sensible) and vapor transfer (latent flux), at 2 cm soil depth.

±2% error of the volumetric soil water content with calibrated probes, so differences between observed and simulated water content could be partly due to the instrument error or to the derived hydraulic properties.

The pronounced differences in soil water content between the upper and the lower soil layers were due to the reduced unsaturated hydraulic conductivity of the dry soil surface layer between the wet soil below and the atmosphere. The hydraulic conductivity versus soil water potential curve is highly nonlinear and, therefore, a small decrease in soil water content corresponded to a large decrease in hydraulic conductivity and liquid water redistribution. According to Darcy's law, the flux is given by the product of the hydraulic conductivity and the water potential gradient, so a small hydraulic conductivity (i.e., a dry soil) implies that the water potential gradient must be large to generate a small water flux. This leads to a steep water potential gradients at the drying front. The numerical instabilities displayed by the numerical code in the lower curve for soil water content are due to the sharper water potential gradient between the two layers, with the deepening of the evaporative front.

The observed diurnal fluctuations in measured soil water content were likely due to (1) real fluctuations of soil water content resulting from vapor flux or (2) possibly due to the soil moisture measuring technique. Diurnal fluctuations of measured soil water content were reported by other authors (Jackson, 1973; Cahill and Parlange, 1998). Jackson (1973) measured water content gravimetrically rather than with electronic probes, and found similar results to this experiment, so it is likely that the soil moisture measuring technique was not the cause of the diurnal fluctuations.

In this field study, soil water content fluctuations were predicted by the model, illustrating it does account for both water vapor flux and condensation. The ECH_2O probe has a maximum temperature sensitivity of $\sim 0.003\ m^3\ m^{-3}\ K^{-1}$ and, therefore, the measured fluctuations seemed to represent real field conditions. Details of the temperature dependence of the ECH_2O probe can be found in Campbell (2006).

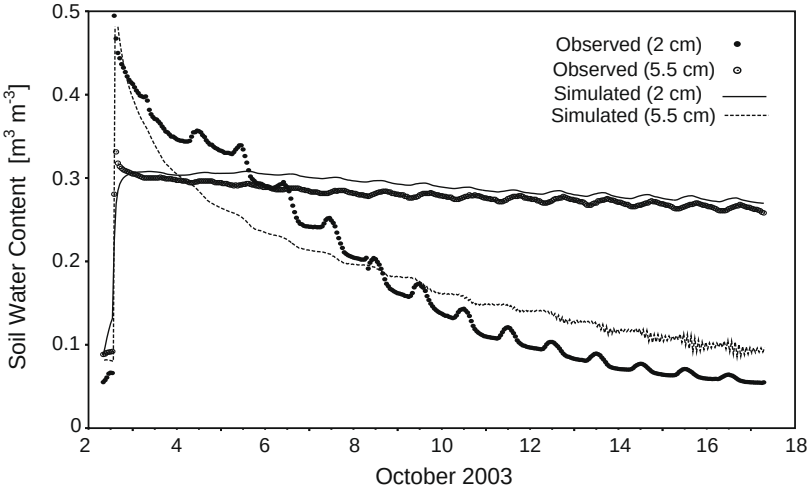

Figure 5 Simulated and measured soil water content for the 2.0 cm and 5.5 cm mean depths versus time.

Soil vapor flux

Fig. 6 shows simulated water vapor flux as a function of time for three measurement depths. Vapor flux decreased from the 2 cm to the 7 cm layer; indicating that water vapor flux is much higher in the layer closer to the surface. This was likely due to (1) higher vapor concentration gradients near the soil and the atmosphere interface, (2) thermal gradients between the lower and the upper soil layers (i.e., water transfer from a warm soil to a cold soil because of temperature and induced increase in the pressure of both liquid and vapor phases), and (3) less liquid water content in pore spaces of the surface layer (Fig. 5), incrementing the air-filled porosity and therefore facilitating vapor flux. Indeed, an important limiting factor for vapor flux is the availability of air-filled pore space for vapor diffusion to occur. Eq. (17) shows that, when the soil is saturated, the air-filled porosity and vapor diffusion are zero, and the vapor diffusion rises with increasing air-filled porosity. In the first few centimeters of soil surface layer, where water content is lower, air-filled porosity and vapor diffusion both increase and facilitate vapor flux, determining the dynamics of the evaporative front.

Since soil vapor flux is proportional to the saturation vapor pressure gradient with depth, it follows that vapor flux experiences diurnal fluctuations due to the reduced soil surface evaporation at night. Water vapor diffuses from deeper in the soil, where it is warmer, to the surface soil where it condenses on the colder soil particles. Since there is less energy available for evaporation into the atmosphere at night and condensation is occurring in the cold surface layer, the liquid water content increases and the vapor pressure typically reaches saturation in the near surface soil layer.

Aerodynamic resistance and soil surface resistance

Different approaches to compute the soil resistance term were analyzed, as shown in Fig. 7.

The Camillo and Gurney (1986) linear model, determined negative resistances at water contents greater than 0.35 $m^3\ m^{-3}$, and high resistances in the dry range, determining unrealistic evaporation rates (as shown in Fig. 9). The Shu Fen (1982) power law model, provided better results since at soil surface water contents (θ_{top}) equal to the saturated water content (θ_s), r_s becomes equal to a minimum value of 37 $s\ m^{-1}$, as described by the equation: $rs = 3.5 * (\theta_s/\theta_{top})^{2.3} + 33.5$. However, the Shu Fen (1982) model, determined an underestimation of evaporation for wet conditions, as described in the next section. The exponential model of van de Griend and Owe provided the best results since the soil resistance reaches a limit at very low water contents, in respect to the Shu Fen (1982) model where, at very low water contents, r_s reaches very large values.

At high water contents, soil surface resistance is low until the water content falls below a lower limit (first stage evaporation). Fig. 8 shows wind speed (top graph) and aerodynamic resistance and soil surface resistance (bottom graph). Aerodynamic resistance depends on wind speed and air temperature, while the soil surface resistance depends on the soil water content of the most superficial soil layer. Wind speed has an important effect on r_v, as indicated during days 9 to 11 of October, where the wind speed increased and the aerodynamic resistance decreased as a consequence. The soil surface resistance displayed the expected increase with time, since soil water content decreases, and displayed the same oscillatory trend displayed by the soil water content. The aerodynamic resistance dominates the overall total resistance until the soil is quite dry. In this experiment the soil surface resistance becomes larger than the aerodynamic resistance approximately on October 16, with surface soil moisture at 0.06 $m^3\ m^{-3}$. The relationship between the resistance values showed again that stage 1 evaporation is mostly controlled by atmospheric parameters (wind speed and temperature), while stages 2 and 3 are determined mostly by the soil surface conditions, in particular by the soil resistance to vapor flow.

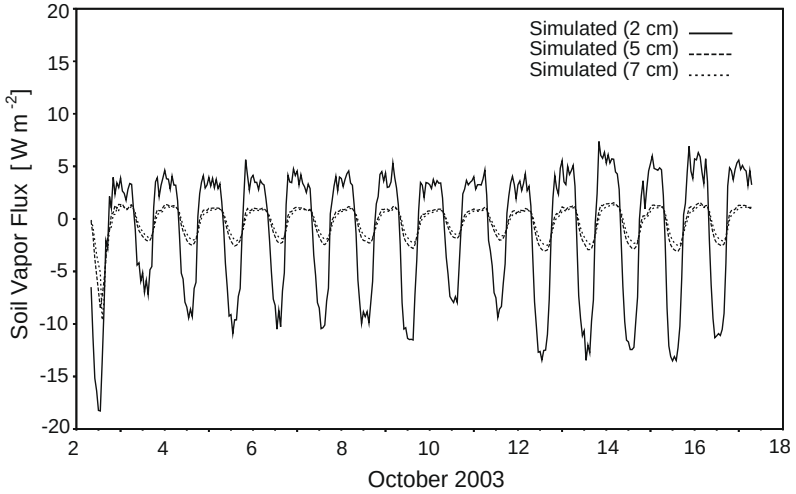

Figure 6 Simulated soil vapor fluxes at 2, 5 and 7 cm depths versus time. Soil water vapor fluxes computed by the model in kg m^{-2} s^{-1} were multiplied by the latent heat of vaporization to express vapor flux in W m^{-2}.

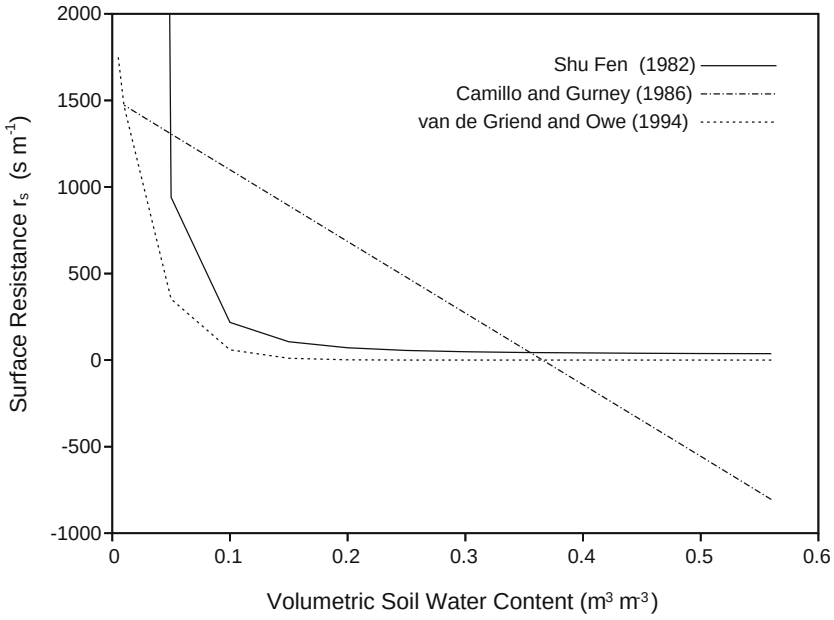

Figure 7 Comparison of different equations for computation of soil surface resistance.

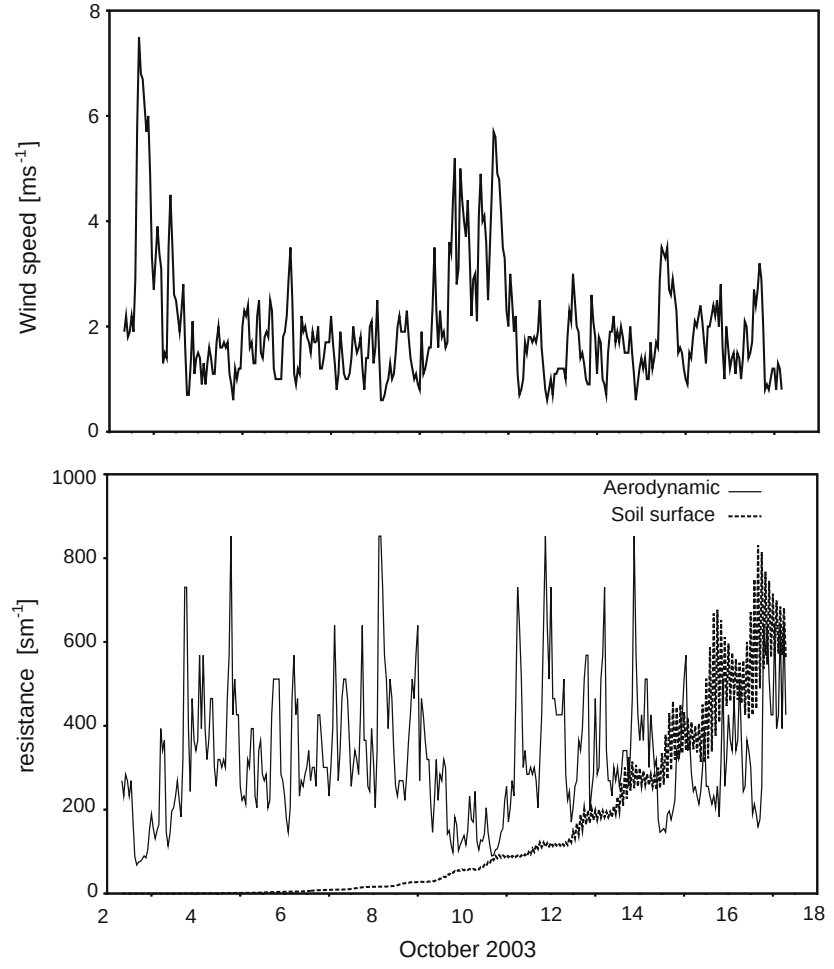

Figure 8 Wind speed, aerodynamic and soil surface resistance as function of time.

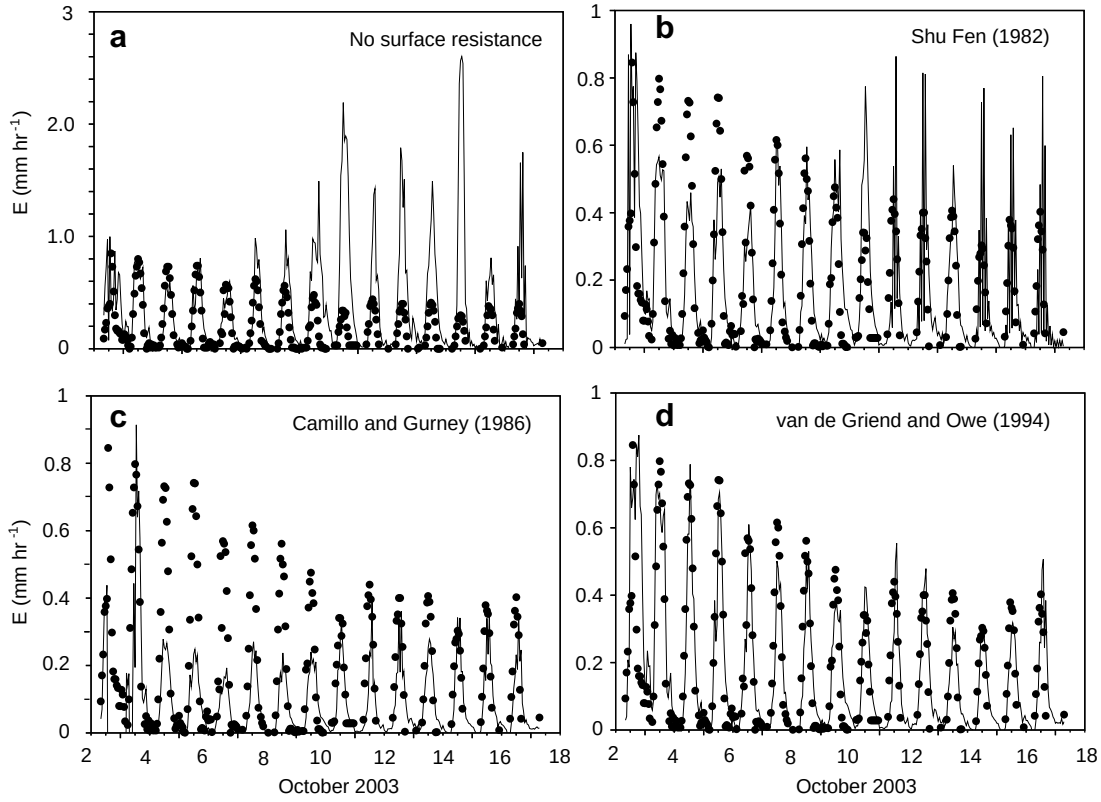

Figure 9 Observed (dots) and simulated (lines) evaporation rates, computed with different equations for the soil surface resistance parameters.

Soil evaporation

Fig. 9 shows simulated and observed soil evaporation from the experiment obtained by using: (a) no soil resistance term (only the aerodynamic resistance), (b) the aerodynamic resistance and the soil resistance, the latter calculated with the Shu Fen (1982) model, (c) the aerodynamic resistance and the soil resistance, with r_s calculated with the Camillo and Gurney (1986) model and (d) the aerodynamic resistance and the soil resistance, the latter calculated with the van de Griend and Owe (1994) model.

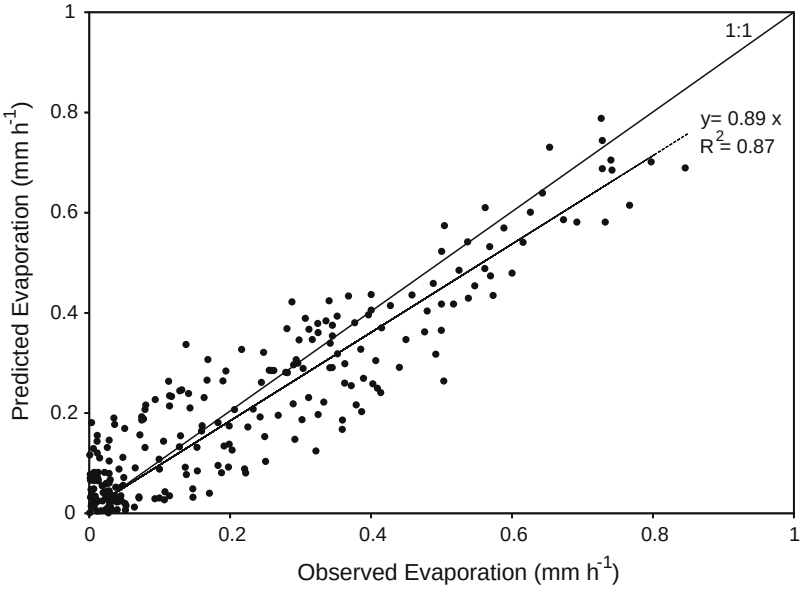

Figure 10 Observed versus predicted evaporation rates, computed with the van de Griend and Owe (1994) equation.

Evaporation computed without the soil resistance term (a), is described reasonably well during phase-1 evaporation (where at high soil water content soil resistance is small), but it is largely overestimated during phase-2 when the soil dries out. These results are in agreement with the works of Shu Fen (1982), Camillo and Gurney (1986) and Kondo et al. (1990) who stressed the importance of considering this resistive term.

Evaporation computed with the aerodynamic and the soil resistance term using the Shu Fen (1982) model (b), provided a much better estimates (note the different *y*-scale) although phase 1 was slightly underestimated and phase 2 was overestimated.

The computation of evaporation with the Camillo and Gurney (1986) linear model showed a large underestimation during phase 1, and a slight underestimation during phase 2. This behavior is explained by the value of r_s as function of soil water content (Fig. 7). The soil surface resistance, which was obtained with the linear equation, displayed bigger values of r_s at high water contents (from 0.4 to 0.1) relative to the Shu Fen (1982) and the van de Griend and Owe (1994) models. This resulted in higher total resistance and hence lower evaporation rates during phase 1.

The van de Griend and Owe (1994) model gave the best estimates of evaporation. The measured soil evaporation (E) was 62.9 mm (over 15 days), while the model predicted 59.3, with an underestimation of 3.6 mm. Good characterization of soil temperature, soil heat flux, and soil water content, however, suggests that the soil compartment was well described by the model and that the discrepancies in cumulative evaporation may be due to difficulties in characterizing the surface boundary layer properties. Although the soil surface was smooth in the experimental area, roughness, convection, the turbulent structure of the wind and other factors may have changed the modeled aerodynamic and surface resistance relative to real values and led to evaporation rate differences. This study confirmed that the soil surface resistance is a key parameter for a correct computation of evaporation. Comparisons between different published equation for its quantification, showed that the van de Griend and Owe (1994) model provided the best estimates. Boundary layer factors can affect vapor transfer more than vapor enhancement mechanisms occurring in the bulk soil (Rose, 1968b) like convective flow due to air expansion. The possibility that convective mass or temperature-induced air flow could affect vapor transport, however, should not entirely be dismissed. The general agreement between the model and observations was good (Fig. 10), having an $R^2 = 0.87$ and a slope = 0.89 through the origin. The RMSE was 0.011 mm h^{-1}.

Conclusions

A numerical model was developed to simulate coupled heat, water vapor, and liquid water flux through soil. The model was tested in field conditions using soil temperature, heat flux, liquid water content, and meteorological data to determine soil evaporation. The model was able to fully calculate the coupled soil mass and energy budget with good agreement between the simulated and the observed data for soil temperature, heat flux and water content as well as for soil evaporation. Comparison of different equations for the soil surface resistance helped to identify the best formulation for this study. In general, the model showed that water vapor transport plays a key role in the soil mass and energy budget and that vapor flux may induce small fluctuations in soil water content near the surface. These results suggest that it is important to consider coupled transport of heat, water vapor and liquid water when computing soil water and energy dynamics in the field, and to obtain a correct quantification of the resistance parameters at the soil—atmosphere interface.

Acknowledgements

This work was supported by the Ministero dell'Universita' e della Ricerca (MiUR), Italy and by the Dept. of Land, Air and Water Research, University of California, Davis, USA. We thank Dr. Khaled M. Bali for his valuable help with the experiment. The computer code, for the solution of coupled fluxes, is available from the authors on request.

References

Ames, W.F., 1992. Numerical Methods for Partial Differential Equations, third edition. Academic Press, San Diego.

Brutsaert, W., Chen, D., 1995. Desorption and the two stages of drying of natural tallgrass praire. Water Resour. Res. 31, 1305—1313.

Buck, A.L., 1981. New equations for computing vapor pressure and enhancement factor. J. Appl. Metereol. 20, 1527—1532.

Cahill, A.T., Parlange, M.B., 1998. On water vapor transport in field soils. Water Resour. Res. 43, 731—739.

Camillo, P.J., Gurney, R.J., 1986. A resistance parameter for bare soil evaporation models. Soil Sci. 141, 95—105.

Campbell, C. S., 2006. Temperature dependence of the ECH_2 O Probe. Application note. Decagon Devices Inc., Pullman, WA, USA. <http://www.decagon.com/instruments/agdownload.html#echo>.

Campbell, G.S., Norman, John M., 1998. An Introduction to Environmental Biophysics, second edition. Springer-Verlag, New York.

Campbell, G.S., and Shiozawa, S., 1992. Prediction of hydraulic properties of soils using particle-size distribution and bulk density data. In: van Genuchten, M.T., Leij, F.J., Lund, L.J. (Eds.), Indirect Methods for Estimating the Hydraulic Properties of Unsaturated Soils. University of California, Riverside, pp. 317—328.

Campbell, G.S., 1977. An Introduction to Environmental Biophysics. Springer-Verlag, New York.

Campbell, G.S., 1985. Soil Physics with Basic, Transport Models for Soil—Plant Systems. Elsevier, Amsterdam, Netherlands.

Campbell, G.S., Jungbauer, J.D., Bidlake, W.R., Hungerford, R.D., 1988. Predicting the effect of temperature on soil thermal conductivity. Soil Sci. 158, 307—313.

Cary, J.W., 1963. Onsanger's relation and the non-isothermal diffusion of water vapor. J. Phys. Chem. 67, 126—129.

Cary, J.W., 1964. An evaporation experiment and its irreversible thermodynamics. Int. J. Heat Mass Transfer 7, 531—538.

Cass, A., Campbell, G.S., Jones, T.L., 1984. Enhancement of thermal water vapor diffusion in soil. Soil Sci. Soc. Am. J. 48, 25—32.

de Vries, D.A., 1963. Thermal properties in soil. In: van Wijk, W.R. (Ed.), Physics of Plant Environment. North Holland Pub. Co., Amsterdam, pp. 210—235.

Feddes, R.A., 1971. Water, heat and crop growth. PhD thesis, Comm. Agric. Univ., Institute of Land and Water Management Research, Wageningen, 184pp.

Flerchinger, G.N., Hudson, C.L., Wight, J.R., 1996. Modeling evapotranspiration and surface energy budgets across a watershed. Water Resour. Res. 32, 2539–2548.

Grismer, M.E., Bali, K.M., Robinson, F.E., 1995. Field scale neutron probe calibration and variance analysis for clay soil. J. Irrig. Drain. Eng. 121, 354–362.

Guo Yu, Q., Ben-Asher, J., Yano, T., Momii, K., 1999. Estimation of soil evaporation using the differential temperature method. Soil Sci. Soc. Am. J. 63, 1608–1614.

Idso, S.B., Reginato, R.J., Jackson, R.D., Kimball, K.B., Nakayama, F.S., 1974. The three stages of drying in a field soil. Soil Sci. Soc. Am. Proc. 38, 831–837.

La Mer, V.K., Healy, T.W., 1965. Evaporation of water: its retardation by monolayers. Science 148, 36–41.

Jackson, R.D., 1973. Diurnal changes in soil water content during drying, in field soil water regime. In: Bruce, R.R. (Ed.), Field Soil Water Regime. 5. SSSA Spec. Publ., pp. 37–55.

Jackson, R.D., Reginato, R.J., Kimball, B.A., Nakayama, F.S., 1974. Diurnal soil–water evaporation: comparison of measured and calculated soil–water fluxes. Soil Sci. Soc. Am. Proc. 38, 861–866.

Jassal, R.S., Novak, M.D., Black, M.D., 2003. Effect of surface layer thickness on simultaneous transport of heat and water in a bare soil and its implications for land surface schemes. Atmos. Ocean 41, 259–272.

Jury, W.A., Letey, J., 1979. Water vapor movement in soil: reconciliation of theory and experiment. Soil Sci. Soc. Am. J. 43, 823–827.

Kondo, J., Saigusa, N., Sato, T., 1990. A parameterization of evaporation from bare soil surface. J. Appl. Meteorol. 29, 385–389.

Morton, K.W., Mayers, D.F., 1994. Numerical Solution of Partial Differential Equations. Cambridge University Press, Cambridge, UK.

Paniconi, C., Putti, M., 1994. Comparison of Picard and Newton iteration in the numerical solution of multidimensional variably saturated flow problems. Water Resour. Res. 30, 3357–3374.

Parlange, M.B., Cahill, A.T., Nielsen, D.R., Hopmans, J.W., Wendroth, O., 1998. Review of heat and water movement in field soils. Soil Tillage Res. 47, 5–10.

Paw U, K.T., Brunet, Y., 1991. A surface renewal measure of sensible heat flux density. In: Proceedings of the 20th Conference of Agriculture and Forest Meteorology, AMS, pp. 52–53.

Paw U, K.T., Qiu, J., Su, H.B., Watanabe, T., Brunet, Y., 1995. Surface renewal analysis: a new method to obtain scalar fluxes without velocity data. Agric. Forest Meteorol. 74, 119–137.

Paw U, K.T., Snyder, R.L., Spano, D., Su, H.B., 2005. Surface renewal estimates of scalar exchange. In: Hatfield, J.L., Baker, J.M. (Eds.), Micrometeorology in Agricultural Systems. ASA Monograph No. 47, ASA-CSSA-SSSA, Madison, WI, pp. 455–483, ISBN: 0-89118-158-X.

Philip, J.R., de Vries, D.A., 1957. Moisture movement in porous materials under temperature gradients. Trans. Am. Geophys. Union 38, 222–231.

Press, W.H., Teukolsky, S.A., Vetterling, W.T., Flannery, B.P., 1992, 2nd ed.Numerical Recipes the Art of Scientific Computing, vol. 5 Cambridge University Press, Cambridge.

Rose, C.W., 1968a. Water transport in soil with a daily temperature wave. I Theory and experiment. Aust. J. Soil Res. 6, 31–44.

Rose, C.W., 1968b. Water transport in soil with a daily temperature wave. II Analysis. Aust. J. Soil Res. 6, 45–57.

Saito, H., Šimünek, J., Mohanty, B.P., 2006. Numerical analysis of coupled water, vapor, and heat transport in the Vadose Zone. Vadose Zone J. 5, 784–800.

Shu Fen Sun, 1982. Moisture and heat transport in a soil layer forced by atmospheric conditions. M.Sc. thesis, University of Connecticut.

Snyder, R.L., Bali, K., Ventura, F., Gomez-Macpherson, H., 2000. Estimating evaporation from bare or nearly bare soil. J. Irrig. Drain. Eng. 126 (6), 399–403.

Snyder, R.L., Pruitt, W.O., 1992. Evapotranspiration data management in California. Water Forum 92 — Irrigigation and Drainage Session. ASCE, New York, NY.

Snyder, R.L., Paw U, K.T., Spano, D., Duce, P., 1997. Surface renewal estimates of evapotranspiration Theory. In: ISHS (Editor), Proceedings of the 2nd International Symposium on Irrigation of Horticultural Crops, vol. 1. Acta Horticulturae.

Snyder, R.L., Spano, D., Paw U, K.T., 1996. Surface renewal analysis for sensible heat flux density. Boundary-Layer Metereol. 77, 259–271.

Spano, D., Snyder, R.L., Duce, P., Paw U, K.T., 1997. Surface renewal analysis for sensible heat flux density using structure functions. Agric. Forest Meteorol. 86, 259–271.

Taylor, S.A., Cavazza, L., 1954. The movement of soil moisture in response to temperature gradients. Soil Sci. Soc. Am. Proc. 18, 351–358.

Tennekes, H., 1973. Similarity laws and scale relations in planetary boundary layers. In: Haugen, D.A. (Ed.), Workshop on Micrometeorology, American Meteorological Society, Boston, MA, pp. 177–216.

van de Griend, A., Owe, M., 1994. Bare soil surface resistance to evaporation by vapor diffusion under semiarid conditions. Water Resour. Res. 30 (2), 181–188.

Ventura, F., Faber, B., Bali, K., Snyder, R.L., Spano, D., Duce, P., Schulbach, K.F., 2001. A model for estimating evaporation and transpiration from row crops. J. Irrig. Drain. Eng. 127 (6), 339–345.

Ventura, F., Snyder, R.L., Bali, K.M., 2006. Estimating evaporation from bare soil using soil moisture data. J. Irrig. Drain Eng. 132, 153–158.

Webb, E.K., 1977. Profile relationships: the log-linear range, and extension to strong stability. Q.J.R. Meteorol. Soc. 96, 67–90.